Applied Catalysis B: Environmental 180 (2016) 65–77

Contents lists available at ScienceDirect

Applied Catalysis B: Environmental

journal homepage: www.elsevier.com/locate/apcatb

# Microporous titania–silica nanocomposite catalyst-adsorbent for ultra-deep oxidative desulfurization

Amin Bazyari[a,c], Abbas A. Khodadadi[a], Alireza Haghighat Mamaghani[a], Javad Beheshtian[b], Levi T. Thompson[c,*], Yadollah Mortazavi[a,*]

[a] Catalysis and Nanostructured Materials Research Laboratory, School of Chemical Engineering, University of Tehran, P.O. Box 11155/4563, Tehran, Iran
[b] Department of Chemistry, Faculty of Sciences, Shahid Rajaee Teacher Training University, P.O. Box 16785-163, Tehran, Iran
[c] Department of Chemical Engineering and Hydrogen Energy Technology Laboratory, University of Michigan, Ann Arbor, MI 48109, USA

ARTICLE INFO

*Article history:*
Received 12 February 2015
Received in revised form 7 June 2015
Accepted 9 June 2015
Available online 10 June 2015

*Keywords:*
Titania–silica
Nanocomposite
Oxidative desulfurization
Dibenzothiophene
DFT

ABSTRACT

High-performance microporous titania–silica ($TiO_2$–$SiO_2$) nanocomposites with different $TiO_2$ loadings of 0–100 wt% were synthesized using a sol–gel method and evaluated for ultra-deep oxidative desulfurization (ODS) of dibenzothiophene (DBT) using *tert*-butyl hydroperoxide (TBHP) as oxidant. The prepared catalysts were characterized by the $N_2$ adsorption–desorption, X-ray diffraction (XRD), Fourier transform infrared spectroscopy (FTIR), high resolution transmission electron microscopy (HR-TEM) and ammonia temperature-programmed desorption ($NH_3$-TPD), and the ODS performances were evaluated in a batch reactor. The effects of titanium loading, calcination temperature, and reaction temperature on the catalyst performance were examined. The activity varied significantly with the amount of titanium in the $TiO_2$–$SiO_2$ nanocomposite with a nearly constant turnover frequency (TOF) of about 24.6 $h^{-1}$. The $TiO_2$–$SiO_2$ nanocomposite containing 50 wt% titania loading (TS-50) with the highest total acidity was an excellent catalyst capable of removing more than 98% of DBT to less than 10 ppmw, after 20 min. DBT was oxidized to DBT-sulfone ($DBTO_2$), a species with higher polarity that could be subsequently adsorbed on the TS-50 and therefore, the nanocomposite acts as both a catalyst and adsorbent simultaneously. The catalysts could be easily regenerated by calcination at 873 K. An empirical kinetic model was employed to interpret the reaction rate data; the apparent activation energy was 43.8 kJ/mol. Density functional theory (DFT) calculations revealed that DBT and TBHP reactants and $DBTO_2$ product were more strongly adsorbed on (0 0 1) surface of β-cristobalite silica than on (1 0 1) surface of anatase titania. The adsorption energy of $DBTO_2$ was larger than DBT on both surfaces.



## 1. Introduction

Environmental concerns are driving refiners to remove the sulfur-containing compounds from transportation fuels [1]. These sulfur compounds react with oxygen during combustion processes in vehicle engines and lead directly to $SO_x$ emission which is one of the major sources of air pollution and acid rain [2,3]. Moreover, sulfur compounds poison the catalysts used in catalytic converters and also corrode combustion engine parts. In order to address these challenges, new specifications for the fuels with regard to their sulfur content have been established in many countries. For instance, in the United States, the sulfur concentrations in diesel and gasoline are limited to less than 15 and 30 ppmw, respectively, according to US EPA regulations [4–6]. Furthermore, the development of fuel cells that consume gasoline and diesel fuels, directly (e.g., solid oxide fuel cells (SOFC)) or indirectly (e.g., proton exchange membrane fuel cells (PEMFC)), necessitates ultra-deep desulfurization to levels less than 1 ppmw for PEMFCs and well below 10 ppmw for SOFCs [7–9].

Catalytic hydrodesulfurization (HDS) is the conventional industrial process for removing sulfur compounds from fossil fuel streams. HDS is highly efficient for eliminating mercaptanes, sulfides, disulfides and some thiophene (T) derivatives [10,11]. However, recent studies report that the performance of this process for removing refractory sulfur compounds typically in diesel fuel such as benzothiophene (BT), dibenzothiophene (DBT) and their derivatives is poor [5,12,13]. In order to produce ultra-low sulfur diesel fuel using current HDS technologies, severe operating conditions including higher temperatures, excessive hydrogen pressures, large volumes of catalyst and/or more active catalysts are required. Achieving these requirements is very costly and also several unde-

* Corresponding authors. Tel.: +98 21 6696 7793; fax: +98 21 6696 7793.
*E-mail addresses:* ltt@umich.edu (L.T. Thompson), mortazav@ut.ac.ir (Y. Mortazavi).

http://dx.doi.org/10.1016/j.apcatb.2015.06.011
0926-3373/

sired side products are formed [14,15]. Therefore, development of alternative or complementary ultra-deep desulfurization processes is of great interest [16].

Oxidative desulfurization (ODS) is considered as one of the most promising methods to obtain ultra-low sulfur fuels. This process has several advantages over conventional HDS processes. ODS can be carried out at atmospheric pressure and low temperatures, without consumption of expensive hydrogen. In addition, the most refractory sulfur compounds to HDS exhibit high oxidation reactivities [12]. In the ODS process, sulfur-containing compounds, in the presence of an oxidant, are oxidized to form sulfoxides and sulfones. These oxidized sulfur compounds have higher polarities than their parent sulfur compounds and the other hydrocarbons and can be removed by various separation processes such as solvent extraction and adsorption. To date, a variety of different oxidizing agents have been studied for the ODS process including $H_2O_2$ [6,10–12,14,15,17], *tert*-butyl hydroperoxide (TBHP) [13,18], $O_2$ [19] and superoxides [20]. $H_2O_2$ due to its low price and significant oxidation property has been widely used with numerous homogenous and heterogeneous catalysts [21–25]. However, $H_2O_2$ is not oil-soluble leading to a biphasic system, which limits the mass transfer and consequently suppresses the rate of the oxidation reaction [19]. In order to avoid these problems, some researchers have proposed to use organic oxidants such as TBHP. Using these oil-soluble oxidizing agents, the ODS process can be conducted in a fixed-bed reactor via a single-phase reaction mixture, making the industrial applications of this approach more feasible [26–28].

Investigations have shown that transition-metal (Ti, Mo, V, W, etc.) composites are active and selective heterogeneous catalysts for the oxidation of sulfur compounds [11,1–15,18,28–31]. Chica et al. studied the activity and stability of Ti-MCM-41 molecular sieves in a continuous fixed-bed reactor and achieved complete oxidation of DBT into DBT-sulfone ($DBTO_2$) [28]. Prasad et al. examined the ODS of 4,6-DMDBT with TBHP on molybdenum oxide supported on alumina, silica–alumina and magnesia–alumina and reported that the $MoO_3/Al_2O_3$–$SiO_2$ catalyst had the best catalytic performance among all the catalysts [13]. Caero et al. investigated ODS on a series of $V_2O_5$ catalysts supported on alumina, silica, niobia, ceria and titania. The best results for a real diesel fuel desulfurization showed an approximately 99% decrease in the initial amount of sulfur [32]. Torres-García et al. conducted both experimental and theoretical studies on the ODS of different thiophenic compounds using $WO_x$–$ZrO_2$ catalysts and found that the surface density of $WO_x$ species strongly affected the catalyst activity [33].

Titanium-containing catalysts have exhibited high catalytic activities for oxidation reactions. For instance, crystalline titanium silicalite-1 (TS-1) has been reported to be a very effective catalyst for oxidation of thiophene, but its catalytic activity for oxidation of BT and DBT is very low due to its small pore size, which hinders the entrance of these bulkier sulfur compounds into the narrow channels [34] where the most active sites are located. Therefore, many efforts have been devoted to prepare new crystalline Ti-containing silica molecular sieves with larger pore sizes, such as Ti-HMS [34], Ti-SBA-15 [35], Ti-SBA-16 [36], Ti-WMS [37], Ti-beta [38], Ti-MWW [39], as catalysts for the ODS of bulky sulfur compounds. However, these materials suffer from relatively low activities and/or poor stabilities [40]. On the other hand, it has been reported in the literature that amorphous mesoporous $TiO_2$–$SiO_2$ mixed oxides are promising catalysts for reactions involving bulky reactants such as epoxidation of α-isophorone [41]. In addition, amorphous $TiO_2$–$SiO_2$ mixed oxides have been shown to have catalytic activity for epoxidation of olefins in the presence of TBHP [42]. Based on these studies, it seems that an amorphous microporous $TiO_2$–$SiO_2$ nanocomposite with a pore size large enough to accommodate the bulky sulfur compounds could be an active catalyst for oxidation of these molecules in presence of TBHP. To the best of our knowledge, there is no report on the ODS of refractory sulfur compounds over amorphous microporous silica–titania nanocomposites with different $TiO_2$ loadings as opposed to several studies published on the crystalline mesoporous silica–titania molecular sieves which contain limited amount of titanium as framework titanium atoms. Therefore, in the continuous search for new catalysts, microporous $TiO_2$–$SiO_2$ nanocomposites may provide alternative catalysts with increased ODS activities for the bulky sulfur compounds such as DBT. If the silica and titania were sufficiently intermixed in the $TiO_2$–$SiO_2$ catalyst, the prepared mixed oxide would take advantage of both titania, probably as the main active component, and silica, for its high thermal stability, excellent mechanical strength and high surface area.

The principal objectives of the present study were to synthesize amorphous microporous $TiO_2$–$SiO_2$ nanocomposites using sol–gel method, and employ them for removing DBT from a simulated fuel made of 2875 ppmw DBT (equivalent to 500 ppmw S) in isooctane by ODS in the presence of TBHP, an oil-soluble oxidant. The effects of titanium loading, calcination temperature, regeneration, and reaction temperature on the ODS performance were examined to establish a structure–function relationship of the microporous titania–silica nanocomposite and provide a basis for optimization of the desulfurization conditions.

## 2. Experimental

### 2.1. Chemicals

All chemicals were used as received without further purification. Tetraethylorthosilicate (TEOS, ≥99%), tetraethylorthotitanate (TEOT, 95%), ethanol (EtOH, ≥99.5%), nitric acid ($HNO_3$, 69 wt%), 1-benzothiophene (BT, ≥98%), dibenzothiophene (DBT, ≥98%), isooctane (≥99%), and aqueous solution of *tert*-butyl hydroperoxide (TBHP, 70 wt%) were all obtained from Merck. 4,6-dimethyldibenzothiophene (4,6-DMDBT, 95%) was purchased from Acros.

### 2.2. Preparation of catalysts.

Microporous $TiO_2$–$SiO_2$ nanocomposites were prepared by a sol–gel method based on the procedure reported elsewhere [43] with some modifications. Sol–gel methods are very effective for the preparation of nano-sized metal oxide materials and possess several important advantages over other methods such as simplicity, molecular scale mixing, and ability to control the textural and surface properties [44–46]. The synthesis procedure was as follows: X mol of TEOS was first mixed with 5X mol of EtOH and stirred at room temperature for 1 h (liquid A). Then a homogenous mixture of $EtOH:H_2O:HNO_3$:TEOT with a molar composition of 30:300:1.8:1 was prepared (liquid B). Nitric acid was added in order to catalyze the sol–gel hydrolysis and condensation reactions. The amounts of TEOS and TEOT were adjusted to produce catalysts with titania loadings ranging from 0 to 100 wt%. The liquid B was added dropwise to the liquid A, and the fully mixed solution was vigorously stirred at room temperature for an additional hour. The prepared sol was stirred at 353 K for a few hours until a wet gel was obtained. The wet gel was dried at 383 K, followed by calcination in static air at different temperatures, i.e., 673, 773, 873, 973 K, for 5 h. The catalyst samples were then pelleted, crushed and sieved to mesh size of 140–230 (63–100 μm). The samples were labeled TS-*x* where *x* is the weight percentage of titania in the nanocomposites.

### 2.3. Characterization of catalysts

X-ray powder diffraction (XRD) patterns of the catalysts were recorded by using a X'Pert Philips Diffractometer with Cu Kα radi-

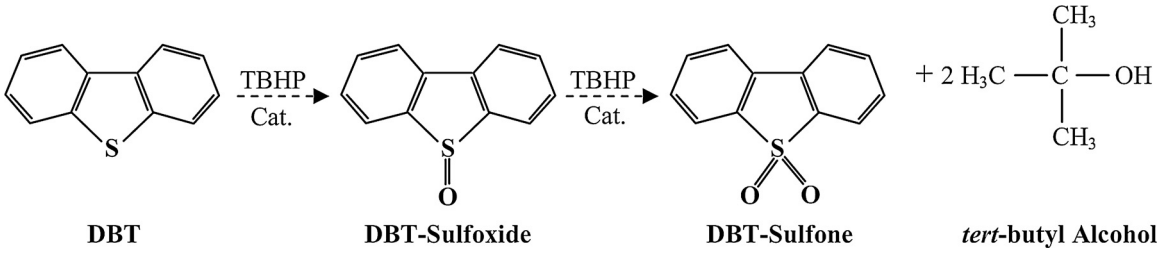


**Scheme 1.** Simplified catalytic oxidation reaction of DBT with TBHP.

ation ($\lambda$ = 1.54056 Å, 40 kV, 40 mA) in a step scanning mode with $2\theta$ between 10° and 65°, and at a scan speed of 1.5°/min. The average crystallite sizes were estimated from the line broadening of the most intense XRD reflections using the Scherrer formula.

The BET surface areas and pore size distributions of the catalysts were measured by analysis of nitrogen isotherms collected at 77 K using a Micromeritics ASAP 2010 apparatus. Before the measurements, the samples (0.2 g) were degassed at 573 K for 1.5 h under vacuum to ensure a clean surface. The BET surface areas were determined from the $N_2$ adsorption at relative pressures of $0.05 < P/P_0 < 0.3$. Pore size distribution was calculated by Barrett–Joyner–Halenda (BJH) method from the adsorption branch of the $N_2$ physisorption isotherms.

Temperature-programmed desorption of ammonia ($NH_3$-TPD) from the samples was conducted using a Quantachrome CHEMBET-3000 apparatus equipped with a TCD detector. In order to evaluate the acidities of the catalysts, adsorption of anhydrous ammonia was carried out at 373 K by exposing 0.2 g of the samples to 20 sccm 5.0 vol% $NH_3$/He gas mixture for 1.5 h. After purging the materials of physically bound $NH_3$ at 373 K, ammonia TPD was performed at a heating rate of 10 K/min from 373 up to 773 K under pure He.

High resolution transmission electron microscopy (HR-TEM) analysis was performed using a JEOL EM-2010F instrument operating at accelerating voltage of 200 kV. The sample powder was ultrasonically dispersed in ethanol and the obtained suspensions were deposited on a lacey carbon film on a copper micro-grid.

Fourier transforms infrared spectra (FTIR) of the catalysts before and after use in the oxidation reaction experiments were recorded on a Bruker Vector22 spectrometer equipped with a DTGS detector. The spectrometer was used in transmission mode with a resolution of 5 $cm^{-1}$ in the range of 700–1800 $cm^{-1}$. The samples for IR measurements were prepared as pellets by embedding the catalyst particles in a KBr matrix with a catalyst:KBr ratio of 2:100. A background spectrum was collected before collection of the samples' spectra.

### 2.4. Measurement of the ODS performance

Evaluation of ODS performance of the catalysts was conducted in a 50-ml three-neck glass batch reactor equipped with magnetic stirrer and condenser. A model fuel with a concentration of 500 ppmw S was prepared by dissolving the appropriate amount of DBT in fixed amount of isooctane. Isooctane was chosen because its boiling point (99 °C) is sufficiently higher than the reaction temperatures tested and it does not vaporize in significant amounts. In a typical reaction experiment, 20 g of the model fuel was heated to three temperatures up to 353 K and then about 0.2 g catalyst and 0.2 g TBHP solution were introduced into the reactor while stirring (~400 rpm). The TBHP:DBT molar ratio of the reaction mixture was adjusted to about 5. As is shown in Scheme 1, the TBHP:DBT stoichiometric molar ratio is 2, but we used TBHP in excess in order to compensate for TBHP mass transfer limitations and decomposition. The reaction progress was monitored by taking samples from the reactor at different reaction times, i.e., after 5, 10, 20, 30, 60 and 120 min. The sulfur concentration of the samples was measured by injecting 1 μl of the samples into a gas chromatograph (GC) purchased from Teif-Gostar company equipped with DB-1 capillary column (30 m long × 0.25 mm I.D. × 1 μm film thickness) and a flame photometric detector (FPD). The injector was used in splitless mode and ultra-high purity helium was used as carrier gas with a flow rate of 1 ml/min. The GC-FPD instrument was calibrated with standard solutions of DBT in isooctane considering the nonlinear response proposed by Ma et al. [47]. The temperature of GC oven was programmed as follows: holding at 453 K for 2 min, raising from 453 to 563 K with a ramp rate of 10 K/min, and finally holding at 563 K for 2 min.

### 2.5. Regeneration of the catalyst

During the course of the ODS reactions, the catalysts became saturated with DBT and the oxidized products and thus, needed to be regenerated. A commonly used regeneration method, i.e., high temperature calcination, was employed for the spent catalyst. In this way the spent catalyst was heated under static air at 873 K for 2 h. The catalytic performance of the regenerated catalyst was then measured in new reaction runs.

### 2.6. Density functional theory calculations

In order to develop a basic understanding of the adsorption of DBT, $DBTO_2$ and TBHP on silica and titania in the course of ODS process, DFT studies were conducted for both oxides. All DFT calculations were carried out using the Quantum-ESPRESSO suite of codes [48] with the Perdew–Burke–Ernzerhof (PBE) generalized gradient approximation (GGA) exchange–correlation functional [49]. A plane-wave expansion with an energy cutoff of 380 eV was used for all calculations. The Brillouin zones of surface supercells were sampled by $6 \times 6 \times 1$ Monkhorst–Pack $k$-point meshes. The electronic self-consistent field was converged to $1 \times 10^{-5}$ eV and the structural optimization was continued until the forces on all atoms were less than 0.03 eV/Å. All calculations were performed spin-polarized.

## 3. Results and discussion

### 3.1. Effect of Ti loading on the ODS performance

In order to examine the effect of titanium loading on the ODS performance, six catalysts with different titania loadings were synthesized: pure silica, TS-10, TS-25, TS-50, TS-75, and pure titania. The performance of each of these catalysts was measured for ODS of the model fuel at 353 K for 120 min. Prior investigations have shown that amorphous $TiO_2$–$SiO_2$ mixed oxides, which have much higher hydrophilicity than crystalline Ti-silicalites like TS-1, are only effective when accompanied by organic hydroperoxides [42]. Accordingly, we decided to use TBHP as the oxidizing agent as opposed to hydrogen peroxide. Commercial diesel fuels always contain small amounts of water which may suppress ODS reac-

**Table 1**
Physicochemical properties of catalytic materials used in ODS experiments.

| Sample[a] | $TiO_2$ (wt%) | $S_{BET}$ ($m^2$/g) | Crystallite size[b] (nm) | Crystalline phase[d] | Total acidity (μmol $NH_3$/g-catalyst) | Acid density (μmol $NH_3/m^2$) |
|---|---|---|---|---|---|---|
| Titania | 100 | 20 | 15.6[c] | A + R | 43 | 2.16 |
| TS-75 | 75 | 145 | 5.8 | A | 438 | 3.02 |
| TS-50 | 50 | 300 | 5.2 | A | 827 | 2.76 |
| TS-25 | 25 | 370 | 3.9 | A | 257 | 0.69 |
| TS-10 | 10 | 390 | Very small/amorphous | Not detected | 154 | 0.40 |
| Silica | 0 | 515 | Amorphous | Amorphous | 9 | 0.02 |

[a] All samples were calcined at 873 K.
[b] Estimated from Scherrer formula ($L = K\lambda/(\beta\cos\theta)$, $K = 0.9$, $\lambda = 1.54056$ Å).
[c] Crystallite size of anatase phase.
[d] A and R stand for anatase phase and rutile phase, respectively.

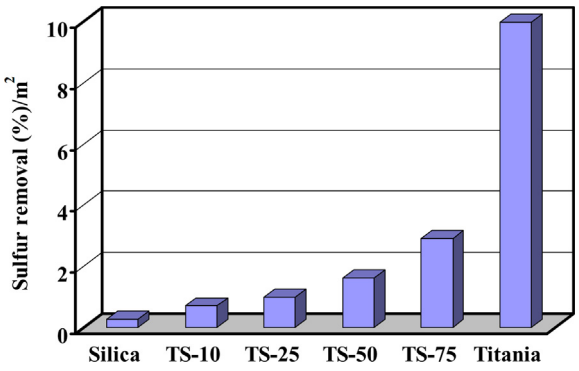


**Fig. 1.** Comparison of the surface-area-normalized ODS performances of different catalysts after 20 min of the reaction. Reaction condition: 20 g of model fuel (2875 ppmw DBT in isooctane), 353 K, 0.2 g catalyst and TBHP:DBT molar ratio of 5.

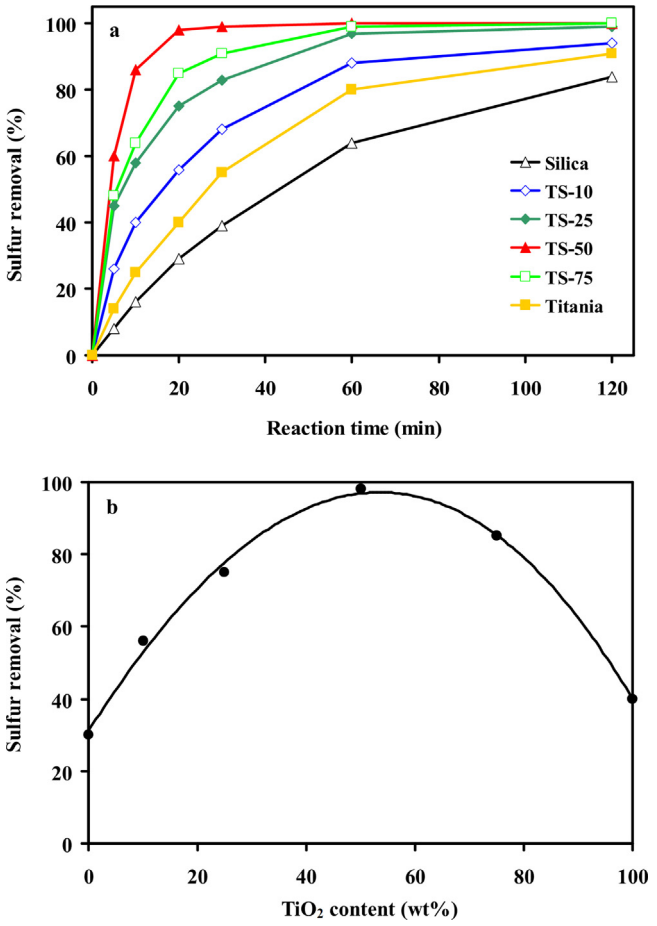


**Fig. 2.** Dependence of the DBT removal vs. reaction time on the loading amount of Ti in $TiO_2$–$SiO_2$ catalysts (a) and comparison of the ODS activities after 20 min of the reaction (b). Reaction condition: 20 g of model fuel (2875 ppmw DBT in isooctane), 353 K, 0.2 g catalyst and TBHP:DBT molar ratio of 5.

tion via covering the surface active sites of the catalyst. Therefore, we used an aqueous solution of TBHP in our reaction system to see if the prepared silica–titania nanocomposites could have acceptable ODS performances in the presence of a small amount of water. The catalysts were used immediately after calcination to avoid the adsorption of more water on the surface.

The percent sulfur removal is defined as the amount of DBT eliminated from the model feed with respect to the initial amount of DBT (multiplied by 100). As is shown in Fig. 1, after 20 min of the reaction, the pure silica catalyst had the lowest sulfur removal percent when normalized to the surface area (i.e., specific activity). The specific activities increased monotonically with the Ti loading. Titania exhibited a 38-fold increase in specific ODS performance as compared to that of silica suggesting that the Ti species were the key components for this reaction.

The overall percent of sulfur removal as a function of reaction time is presented in Fig. 2a. Despite having the highest surface area of ~515 $m^2$/g (see Table 1) silica had the lowest overall desulfurization activity. Titania, with the lowest surface area of ~20 $m^2$/g, performed better than silica. However, all the $TiO_2$–$SiO_2$ nanocomposite catalysts were more active than silica and titania for the ODS reaction and had higher overall sulfur removal rates. A comparison of the overall activities of the catalysts after 20 min of the reaction is shown in Fig. 2b. Overall desulfurization rates increased in the following order: pure silica < pure titania < TS-10 < TS-25 < TS-75 < TS-50. With increasing Ti loading, the measured sulfur removal increased at first and then decreased after passing through a maximum value.

The results suggest that the key factors affecting the activity of $TiO_2$–$SiO_2$ nanocomposite catalysts are the surface area, titania dispersion and loading of Ti. In order to better understand the performance of $TiO_2$–$SiO_2$ nanocomposites in the desulfurization process, three control experiments were conducted on the model fuel: (1) desulfurization over TS-50 in the absence of TBHP; (2) desulfurization with TBHP in the absence of TS-50; and (3) desulfurization over TS-50 in the presence of TBHP. The results for these comparative experiments are presented in Table 2. Results from experiment (1) indicate that TS-50 can, in absence of the oxidant, act as adsorbent for DBT and achieve a total desulfurization of 35%. On the other hand, the amount of sulfur removed as DBT via adsorption in experiment (1) plus the amount of sulfur in the form of $DBTO_2$ from experiment (2) is always well less than 500 ppmw S. Comparing the results from experiments (1) and (2) with that of experiment (3) indicates that TS-50 functioned both as an adsorbent and catalyst. The oxidation of DBT would produce $DBTO_2$ which is more polar and more likely to be adsorbed on the surface of TS-50. It should be noted that experiment (2) was performed at a TBHP:DBT molar ratio of 30, however, in experiment (3) the TBHP:DBT molar ratio was 5. Song and Ma suggested that a combi-

**Table 2**
Comparative experiments with/without oxidant and with/without catalyst.

| Entry | Catalyst and/or oxidant | Sulfur concentration[e] (ppmw S) | | | | Total desulfurization (%) |
|---|---|---|---|---|---|---|
| | | DBT | | $DBTO_2$ | | |
| | | 20 min | 120 min[f] | 20 min | 120 min | |
| 1[a,b] | TS-50 | 350 | 325 | 0 | 0 | 35 |
| 2[a,c] | TBHP | 400 | 350 | 100 | 150 | 0 |
| 3[a,d] | TS-50 and TBHP | <10 | <5 | 0 | 0 | >99 |

[a] Feed: DBT (500 ppmw S) + isooctane, reaction temperature: 353 K.
[b] Catalyst: 0.2 g of TS-50.
[c] TBHP:DBT(molar ratio) = 30.
[d] TBHP:DBT(molar ratio) = 5, catalyst: 0.2 g of TS-50.
[e] Concentration of sulfur remaining in the reaction mixture after removing the catalyst particles.
[f] Overall reaction time: 120 min.

nation of oxidation and adsorption processes in one material could lead to a considerable ODS efficiency when compared to using independent oxidation or adsorption processes [1].

The higher overall and specific activities of pure titania compared to pure silica demonstrated that the former catalyst had more active sites or a higher active site density. Considering results for the $TiO_2$–$SiO_2$ nanocomposite catalysts, increasing the Ti loading may have increased the density of active sites up to TS-50; further increases were likely by a sharp decrease in the surface area and may have resulted in a decrease in the number of surface active Ti species.

It worth mentioning that the catalysts for ODS were used immediately after calcination at 873 K because our experiments showed that high temperature thermal treatment of pure titania and $TiO_2$–$SiO_2$ nanocomposites in air improved the sulfur removal capacity significantly compared to the samples that were simply dried at 383 K. Nair and Tatarchuk reported similar effects on the sulfur removal capacity of $TiO_2$ and $\gamma$-$Al_2O_3$ adsorbents. The calcined $TiO_2$ was nearly 4 times more active than the dried sample [50]. They concluded that calcination generated active centers on the $TiO_2$ and $\gamma$-$Al_2O_3$ supports. Calcination at 873 K can remove water and strongly coordinated hydroxyl groups from the surface to a large extent, thus exposing Lewis acid sites or increasing the density of single surface hydroxyl groups, which are believed to be the active centers for adsorption and possibly the subsequent ODS reactions. The DBT family of compounds can display some Lewis base character due to the lone electron pairs on the sulfur atom. Therefore, they can be adsorbed on the active sites of the $TiO_2$–$SiO_2$ nanocomposites via a Lewis acid–base type interaction. This acid–base interaction can facilitate the adsorption of DBT and its oxidation products on the catalyst surface, which consequently improves the ODS efficiency [51–54]. These results suggest that acidity can be an important factor affecting the $TiO_2$–$SiO_2$ nanocomposite catalysts in the catalytic ODS process.

The specific surface areas ($S_{BET}$), crystalline phases and titania crystallite sizes are listed in Table 1. All of the samples were calcined at 873 K. As it can be seen, the surface areas were strongly dependent on the titania content and increased from 20 $m^2$/g for pure titania to 515 $m^2$/g for the pure silica. The decrease in surface area with increasing Ti content can partly be explained by the higher atomic mass of Ti, but most of the surface area loss can be attributed to an increased contribution of the pure titania character. Considering the calcination temperature, the $TiO_2$–$SiO_2$ nanocomposites represent considerably high surface areas that can be ascribed to the influence of the silica. Silica can act as a support for the titania and facilitates achieving and maintaining a large surface area.

Pure titania nanostructures exhibit poor thermal stabilities, a property that plays an important role in many potential applications of nanostructured materials [55]. During the course of the sol–gel and high temperature calcination, surface hydroxyl (OH)/alkoxyl (OR) groups combine to release water and form

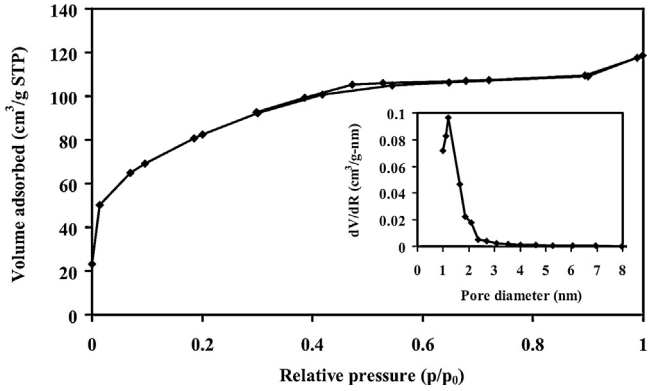


**Fig. 3.** $N_2$ adsorption–desorption isotherms and corresponding pore size analysis of TS-50.

Ti—O—Ti linkages. Therefore, the titania nanoparticles aggregate into large clusters, the surface area concomitantly decreases, and the anatase phase transforms into the rutile phase [56]. In the presence of silica nanoparticles, which are presumably rich with surface hydroxyl/alkoxyl groups, similar condensation reactions can occur between the two different oxides, which produce dissimilar oxide interfaces. At the interfaces, some Ti atoms randomly substitute for Si atoms in the silica framework to form tetrahedral Ti sites. The interaction between the tetrahedral Ti species and the octahedral Ti sites in the anatase phase is thought to hinder the sintering and transformation from anatase to rutile. In other words, the silica framework locks the Ti—O bridges at the interface with the titania domains and prevents severe sintering and reduction of surface area in the $TiO_2$–$SiO_2$ nanocomposites compared to pure titania. These inferences are confirmed by FTIR results.

The $N_2$ adsorption–desorption isotherms and pore size distribution for TS-50, the catalyst with the highest overall desulfurization rate and capacity, are shown in Fig. 3. This material produced a type I isotherm according to IUPAC classification. This type of isotherm is characteristic of a microporous material. The inset of Fig. 3 illustrates the pore size distribution. Monomodal microporosity with a narrow pore size distribution with maximum at 1.2 nm can be observed. This pore size is large enough to allow DBT molecules, with critical diameter of 8 Å [57] to diffuse into the pores where most of the active sites for ODS/adsorption are located. On the other hand the pores are not too wide to allow DBT and its oxidation products to leave the pores without being affected by the active sites. Molecules adsorbed in micropores are subject to stronger adsorption energies owing to the compound interactions with pore walls. Everett and Powl [58] calculated adsorption energies as a function of pore diameter based on the Lennard–Jones potential model, and found that for cylindrical pores having diameters equal or less than five fold of the size of adsorbate molecules, the adsorption

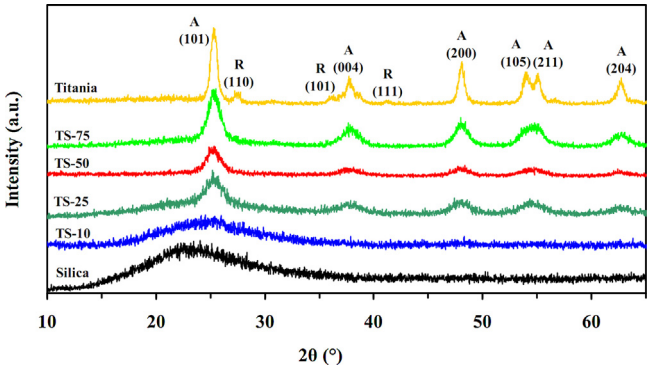


**Fig. 4.** XRD patterns of silica, titania and $TiO_2$–$SiO_2$ nanocomposite catalysts prepared by the sol–gel method and calcined at 873 K.

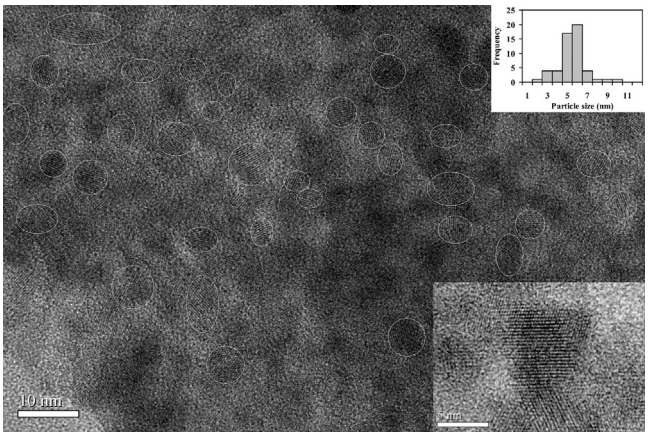


**Fig. 5.** HR-TEM image of TS-50.

energies increased with decreasing pore size. Pores with sizes that were three times or less the size of the adsorbate molecules possessed significantly increased interaction potentials, and as pore size approached that of the adsorbate, interaction potentials were calculated to become more than five times those on a flat surface. The critical diameters of the DBT and $DBTO_2$ molecules are less than but similar to the pores size of TS-50 with diameters of 1.2 nm.

In order to understand how the titania content improved the desulfurization performance of the $TiO_2$–$SiO_2$ nanocomposites, the materials were characterized using XRD. The XRD patterns of pure titania, $TiO_2$–$SiO_2$ nanocomposites, and pure silica and their crystalline properties are shown in Fig. 4 and Table 1. As it can be seen for pure titania, in the absence of silica, calcination at 873 K resulted in a mixture of anatase and rutile crystalline phases. No diffraction peaks for the crystalline silica phase were observed in any of the samples, indicating that the silica was amorphous or highly dispersed. For the nanocomposites with titania content less than 25 wt%, i.e., TS-10, only features typical of amorphous structures were observed. This demonstrates that atomically mixed $SiO_2$–$TiO_2$ oxides, amorphous/disordered phase of titania or highly dispersed crystalline phases of titania on silica can be obtained at a titania content between 10 and 25 wt%. This is in agreement with the previously reported results that the maximum titania solubility concentration in amorphous silica framework is 15 wt% [42,59]. At higher Ti contents, the fraction of tetrahedral Ti atoms associated with Ti—O—Si linkages decreased and octahedral Ti atoms associated with the crystalline phases of titania tended to form a separate phase. The presence of silica significantly enhanced the thermal stability of the anatase phase so that the transformation of anatase to rutile was suppressed at 873 K and all the $TiO_2$–$SiO_2$ nanocomposite catalysts contained anatase as the only titania crystalline phase. Anatase is believed to perform better than rutile for sulfur adsorption from liquid fuels [53]. The high thermal stability enables it to perform thermal treatment on the $TiO_2$–$SiO_2$ nanocomposite catalysts at high temperatures when necessary, e.g., regeneration of spent catalysts, without any significant sintering of the nanodispersed Ti active species and loss of the surface area. The anatase crystallite sizes of the Ti containing samples were estimated by the Scherrer formula using the broadening of the (1 0 1) reflection peak (see Table 1). The anatase crystallite size decreased sharply from 15.6 nm to 5.8 nm with increasing silica content up to 25 wt%. When the silica content was more than 25 wt%, there was no significant change in the titania crystallite sizes with changing the silica content. This result is consistent with some portion of silica inhibiting the growth of anatase crystallites.

The HR-TEM image of TS-50 is shown in Fig. 5. The average particle size of titania (5.0 nm) was consistent with the crystallite size estimate obtained from XRD. Due to differences in the surface energy and surface stress, small crystallite size is thermodynamically in favor of anatase. Therefore, in addition to the strong bonding between titania and silica at the interface, the small crystallite sizes for the $TiO_2$–$SiO_2$ nanocomposites should contribute to inhibiting transformation from anatase to rutile [60]. This would lead to improvements in the desulfurization performances of the $TiO_2$–$SiO_2$ nanocomposites. As the titania loading in the $TiO_2$–$SiO_2$ nanocomposites increased from 10 to 50 wt%, the desulfurization performance also increased. However, the functionality of the nanocomposites decreased at 75 wt% of titania. Therefore, the desulfurization performances of the prepared catalysts seem to be dependent on the joint function of the dispersion of titanium active species, titanium loading and $S_{BET}$.

In order to better clarify how the presence of silica can improve the dispersion of Ti active species and the ODS performance, the pure titania, $TiO_2$–$SiO_2$ nanocomposites, and pure silica materials were characterized using FTIR. The spectra in the region of 1800–700 $cm^{-1}$ are depicted in Fig. 6a. According to the literature the peaks at 810–800 $cm^{-1}$ correspond to the symmetric stretching of Si—O—Si, 1105–1080 $cm^{-1}$ to asymmetric Si—O—Si vibration, 960–940 $cm^{-1}$ to stretching vibration of Si—O—Ti, ~1450 $cm^{-1}$ to stretching vibration of Ti—O—Ti, and 1650–1620 $cm^{-1}$ to bending vibration of OH groups [42]. In all the IR spectra, the bands at 1628 $cm^{-1}$ were assigned to the hydroxyl groups. The intensity of this band increased with the titania content for the $TiO_2$–$SiO_2$ nanocomposites up to 50 wt% and then decreased. It is generally accepted that titania strongly retains adsorbed undissociated water due to the strong Lewis acidity of the coordinatively unsaturated $Ti^{4+}$ surface sites [60]. The increased hydroxyl density could be taken as evidence of a higher amount of Ti surface species in TS-50 compared to pure titania and the other $TiO_2$–$SiO_2$ nanocomposite catalysts. The IR bands observed at 1450 $cm^{-1}$ were attributed to Ti—O—Ti linkages in $TiO_2$ nanoparticles. The TS-75 material shows a more intense peak at 1450 $cm^{-1}$ compared to the other $TiO_2$–$SiO_2$ nanocomposites, implying that the Ti atoms preferred an octahedral configuration over tetrahedral coordination in the silica framework. The peaks centered at ~800 $cm^{-1}$ and 1080 $cm^{-1}$ are representatives of Si—O—Si linkages in the silica framework. As expected, the intensity of these peaks increased with increasing Si content of the samples. The band at 940 $cm^{-1}$ demonstrated the incorporation of titanium into the silica framework for the $TiO_2$–$SiO_2$ nanocomposites [42]. The higher the Si content for the $TiO_2$–$SiO_2$ nanocomposites, the more intensive this peak was and this was opposite the behavior for the Ti—O—Ti band. The very small peak observed for pure $SiO_2$ in this region was ascribed to the stretching vibration of free silanol groups at the surface, which overlapped with the Ti—O—Si peaks [61]. These results clearly define how changing the titanium

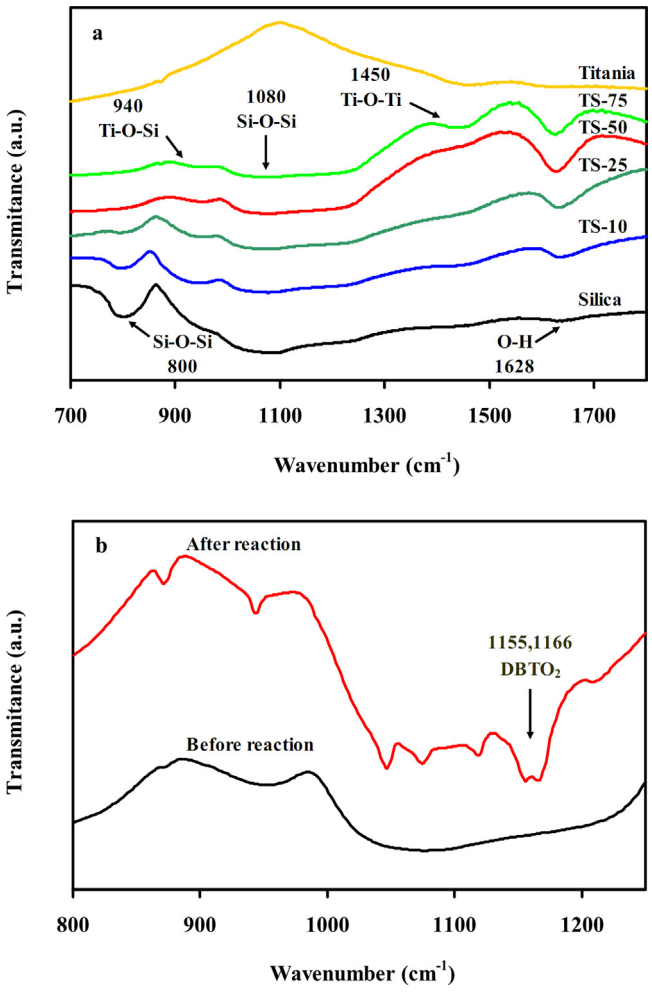


**Fig. 6.** FTIR spectrum of the silica, titania and $TiO_2$–$SiO_2$ nanocomposite catalysts prepared by the sol–gel method and calcined at 873 K (a) and comparison of the FTIR spectrum for TS-50 before and after 120 min of the ODS reaction (b). Reaction condition: 20 g of model fuel (2875 ppmw DBT in isooctane), 353 K, 0.2 g catalyst and TBHP:DBT molar ratio of 5.

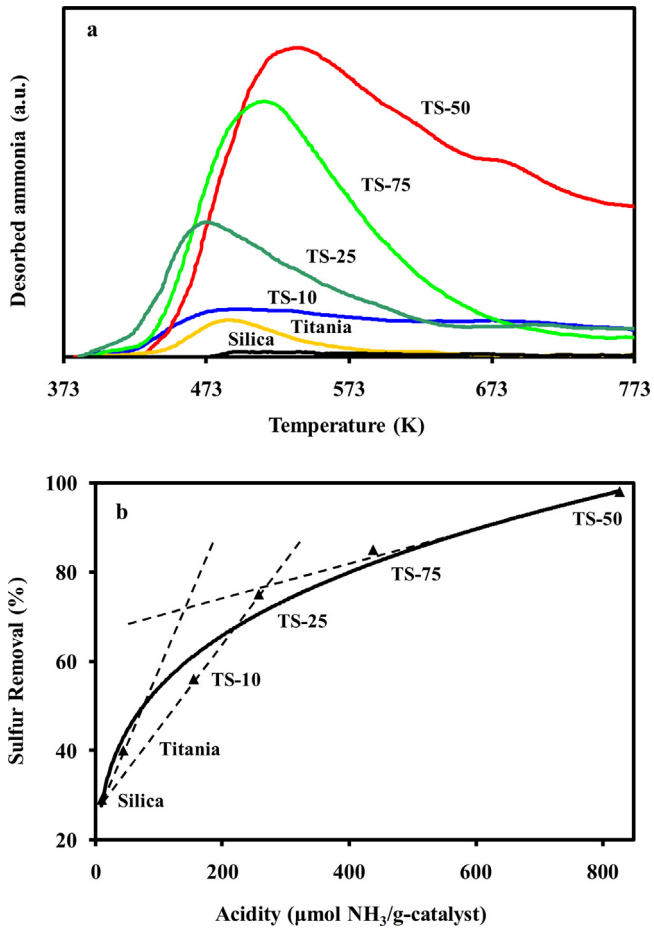


**Fig. 7.** $NH_3$-TPD profiles of the silica, titania and $TiO_2$–$SiO_2$ nanocomposite catalysts prepared by the sol–gel method and calcined at 873 K (a) and the ODS performance after 20 min of the reaction as a function of the acidity of the catalysts (b). Reaction condition: 20 g of model fuel (2875 ppmw DBT in isooctane), 353 K, 0.2 g catalyst and TBHP:DBT molar ratio of 5.

content in the $TiO_2$–$SiO_2$ nanocomposites influence the structure in atomic scale. Based on the BET, XRD, HR-TEM and FTIR results, the $TiO_2$–$SiO_2$ nanocomposites synthesized in this study ($10 \leq TiO_2$ wt% $\leq 75$) were amorphous microporous silica frameworks on/in which a fraction of anatase titania nanoparticles/Ti atoms were welded/incorporated via Ti—O—Si bindings.

FTIR spectra (1250–800 $cm^{-1}$) of the TS-50 material before and after ODS reaction are shown in Fig. 6b. The peaks at 1156 and 1166 $cm^{-1}$ after the ODS reaction both originate from the -$SO_2$- functional group present in the DBT-sulfone ($DBTO_2$), an oxidation product of DBT [27]. This result demonstrates both the ability of the catalyst to oxidize DBT molecules to $DBTO_2$ and its adsorption ability. Analogous "one-pot" ODS operation have recently been reported by Dou and Zeng using $MoO_3/SiO_2$ as catalyst-adsorbent system [62]. No sign of DBT-sulfoxide, DBTO, was seen in the FTIR spectra after the reaction. This result suggests that DBT-sulfoxide formation or its elimination from the active site surface [33] is the rate-determining step.

In order to investigate why TS-50 exhibited much better ODS performance, TPD of adsorbed ammonia was conducted on pure silica, pure titania and $TiO_2$–$SiO_2$ nanocomposites. The amount and strength of the surface acid sites on these catalysts can be deduced. The area under the $NH_3$-TPD profile represents the amount of acid sites whether Brønsted or Lewis, while the temperature of the maxima of the desorption profile are indicative of the strength of the acidic sites. The $NH_3$-TPD profiles of the catalysts are shown in Fig. 7a and the results are listed in Table 1. Pure silica showed negligible acidity, adsorbing only a small amount of ammonia through H-bonds [63], which was easily desorbed. Pure titania has ~5 times more acid sites than pure silica and a maximum desorption at about 479 K. IR spectrum of adsorbed ammonia on pure titania demonstrates that pure titania only possesses Lewis acidity and the hydroxyl groups on pure titania are not capable of protonating ammonia [61]. It can be seen that the acidic properties of $TiO_2$–$SiO_2$ nanocomposites were quite different from that of either pure titania or pure silica. With the increase of the Ti content up to 50 wt%, the number of acid sites increased, which can be ascribed to the increase in the exposed Ti species. The ammonia desorption peaks shifted to higher temperatures, indicating that the adsorption strengths increased with the Ti content. The addition of more Ti resulted in a decrease in the acidity of the sample TS-75. This could be due to the reduction in $S_{BET}$, which in turn results in a decrease in acid site generation. Imamura et al. investigated the acidity of $TiO_2$–$SiO_2$ as a function of Ti content. The acidity increased with Ti content and reached a maximum at a Ti loading of 60 mol%, and then decreased sharply with further increase in Ti loading [64]. Kobayashi et al. reported that $TiO_2$–$SiO_2$ mixed oxides prepared by coprecipitation technique and with different amounts of Ti showed a maximum acidity at Ti:Si molar ratio of 1 [65]. These results are in good agreement with those obtained in the present

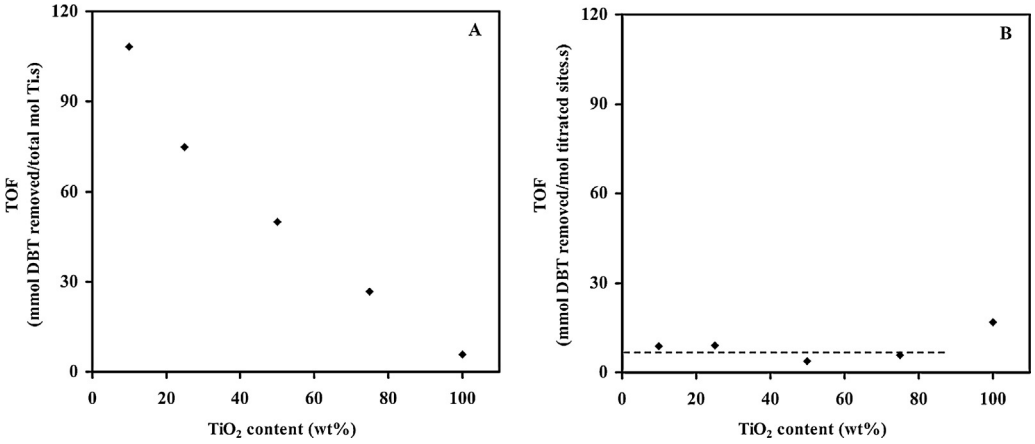


**Fig. 8.** Initial turnover frequencies vs. loading amount of Ti in catalytic ODS of DBT with TBHP on titanium containing samples. TOF is calculated as mmole DBT removed per total mol Ti (A) and per titrated sites (B) per second.

study. It could be concluded that optimal mixing of the two oxides can lead to a considerable increases in the number and strength of acid sites, which can play important roles in catalysis/adsorption performance of the $TiO_2$–$SiO_2$ nanocomposites.

It should be mentioned that there is no consensus in the literature regarding the type, amount and strength of surface acid sites for $TiO_2$–$SiO_2$ mixed oxides. For instance Liu et al. proposed that new Brønsted acid sites are created when titania and silica form Ti—O—Si chemical bonds [66] and Davis and Liu proposed that Brønsted acidity is generated when hydroxyl groups balance the charge imbalance that occurs in Ti—O—Si bonds when Ti atoms isomorphously substitute for the tetrahedral Si atoms in the $TiO_2$–$SiO_2$ mixed oxides [61]. Recent reports by Notari et al. and Hu et al. indicated that only Lewis acidity, and not Brønsted acidity, was present on the surface of high purity amorphous $TiO_2$–$SiO_2$ mixed oxides [67,68]. Regarding the density and strength of surface acid sites, it has been reported that increasing the silica content in the amorphous $TiO_2$–$SiO_2$ mixed oxides decreases the surface acidity, while others have reported the opposite. One can conclude that the acidic properties of $TiO_2$–$SiO_2$ nanocomposites depend largely on the synthesis method and chemical composition, which may govern the Ti—O—Si bond formation, the degree of surface hydroxylation and $TiO_2$ particle size as discussed above.

The ODS performance of the catalysts, after 20 min of the reaction, as a function of their acidity is shown in Fig. 7b. Regardless of the type of acid sites, the results clearly indicate that active sites for ODS/adsorption of DBT molecules are centered on acid sites. A comparable relationship between the acidity and DBT oxidation activity has been reported for the $H_2O_2$–$WO_x/ZrO_2$ catalytic system [69]. The declining slope of the curve shows a decrease in the fraction of $NH_3$ (critical diameter of 3.6 Å)-titrated surface active sites which are accessible to bulky DBT molecules (8 Å). Considering the comparable pore sizes of the microporous $TiO_2$–$SiO_2$ nanocomposites with the critical diameter of DBT molecule this is not unexpected. Materials with different acidic properties follow similar trends with different slopes. This behavior could not most likely be attributed to the different intrinsic reactivities of the active sites. It is worth mentioning that pure $TiO_2$ is nonporous with all the active sites on the external surface and accessible to the reactants, and thus the slope for it is the largest. In order to further clarify this behavior, initial rates of DBT removal (displayed as TOF) after 5 min of the ODS reaction as a function of total Ti loading and surface $NH_3$-titrated sites are shown in Fig. 8A and B, respectively. Fig. 8A shows the dramatic effect of the titania content on the DBT removal performance. The lower the Ti content, the higher the number of DBT molecules removed per Ti atom. This result may mislead one to conclude that the rate of ODS reaction is greater on the catalyst with the lowest titania content. On the other hand, Fig. 8B reveals that this reaction is relatively insensitive to the surface structure of the different $TiO_2$–$SiO_2$ catalysts when normalized by surface sites titrated by $NH_3$ and shows an average turnover frequency (TOF) of 6.84 (mmol DBT removed/mol surface titrated sites/s). Comparing Fig. 8A and B shows that what is changed as a function of Ti loading is the fraction of binding sites rather than their intrinsic reactivity. $TiO_2$–$SiO_2$ nanocomposites with different surface areas and perhaps different pore size distribution, which consequently may lead to different diffusional limitations, have slightly different ratios of surface sites titrated by small $NH_3$ molecules to those accessible to bulky DBT molecules. This could explain the slightly different TOFs for the different nanocomposites.

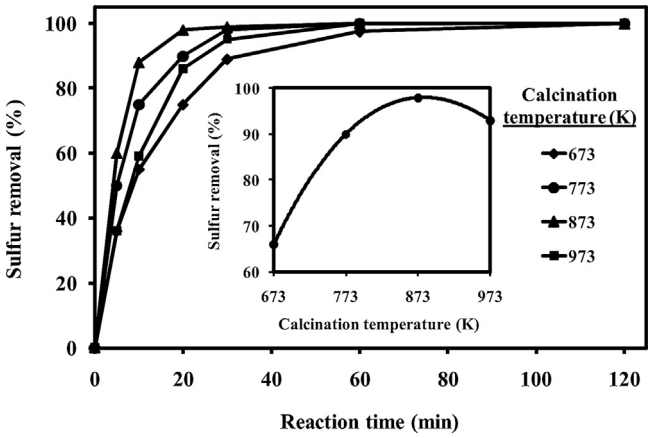


**Fig. 9.** Dependence of the DBT removal vs. reaction time on the calcination temperature of TS-50 (inset shows the DBT removal vs. calcination temperature over TS-50 after 20 min of the reaction). Reaction condition: 20 g of model fuel (2875 ppmw DBT in isooctane), 353 K, 0.2 g catalyst and TBHP:DBT molar ratio of 5.

Since TS-50 shows the best desulfurization performance among all the catalysts, the remaining experiments were carried out on TS-50.

### 3.2. Effect of calcination temperature

Results for the removal of sulfur from the model fuel over TS-50 catalyst calcined at different temperatures as a function of reaction time is presented in Fig. 9. It is clear that the calcination temperature significantly affects the performance of TS-50 especially during short reaction times (inset of Fig. 9) which is practically impor-

**Table 3**
Initial rates ($-r_{DBT}$) and apparent pseudo-first-order apparent rate constants ($k'_{ODS}$) of DBT oxidation evaluated for different periods.

| Period no. | $mol_{DBT}$ ($\times 10^{-4}$)[a] | $C_{DBT}$ ($\times 10^{-3}$ mol/lit)[b] | $k'_{ODS}$ ($\times 10^{-3}$ $s^{-1}$)[c] | $-r_{DBT}$ ($\times 10^{-5}$ mol/lit/s)[d] |
|---|---|---|---|---|
| 1 | 1.25 | 4.31 | 3.0 | 1.29 |
| 2 | 1.38 | 4.76 | 2.7 | 1.28 |
| 3 | 2.19 | 7.56 | 1.2 | 0.90 |

[a] Initial number of moles of DBT in the reaction mixture is $3.125 \times 10^{-4}$.
[b] Initial concentration of of DBT in the reaction mixture is $10.78 \times 10^{-3}$ mol/lit.
[c] $k'_{ODS} = \ln(C_{DBT,0}/C_{DBT,t})/t$. Initial rates and rate constants were evaluated after 5 min of ODS reaction.
[d] $-r_{DBT} = k'_{ODS} \times C_{DBT}$.

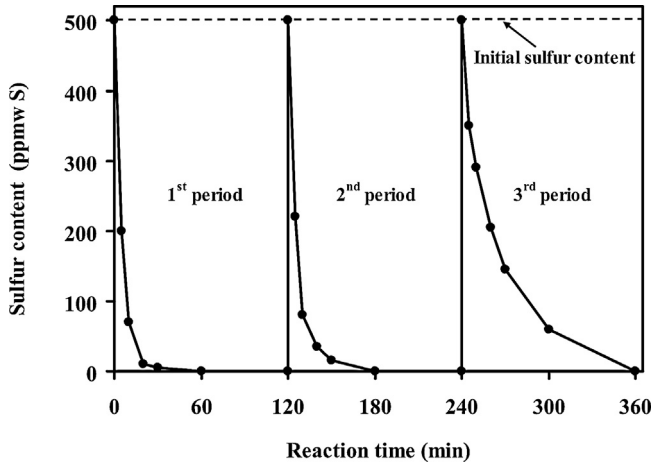


**Fig. 10.** Periodic ODS performance of TS-50. Reaction condition: 20 g of model fuel (2875 ppmw DBT in isooctane), 353 K, 0.2 g catalyst and TBHP:DBT molar ratio of 5.

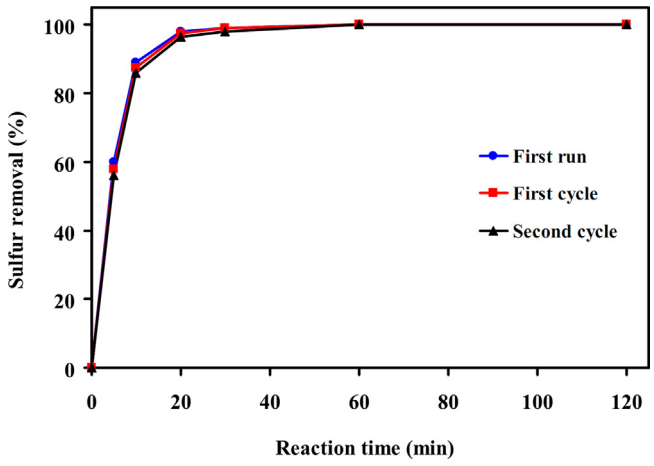


**Fig. 11.** Regeneration study of TS-50. Two regeneration cycles have been carried out. Each regeneration step consisted of the high temperature oxidation of the catalyst at 873 K after ODS reaction. Reaction condition for each step: 20 g of model fuel (2875 ppmw DBT in isooctane), 353 K, 0.2 g catalyst and TBHP:DBT molar ratio of 5.

tant. As can be seen from Fig. 9, the ODS efficiency improved with increasing the calcination temperature up to 873 K. However, further increases led to a reduction in desulfurization performance. The surface areas for TS-50 calcined at 673, 773, 873 and 973 K were 412, 334, 300 and 238 $m^2/g$, respectively. TGA analysis (not shown for the sake of brevity) shows that low calcination temperatures are not adequate to completely decompose the organic residues in the nanocomposite or remove the strongly coordinated hydroxyl groups, which could block surface active sites. On the other hand, excessive calcination temperatures (973 K) result in decreased surface areas.

### 3.3. Evaluation of catalyst stability

Although it is expected that TS-50 will lose its activity during the course of the ODS reaction, due to the adsorption of DBT and $DBTO_2$, but it appears that this catalyst preserves satisfactory performance for more than one batch of the reaction mixture before it needs to be regenerated. Therefore, in order to examine the stability of the TS-50, we designed a periodic ODS experiment in which the spent TS-50, at the end of the first 120 min, was brought into contact with the second and third batch of the same reaction mixture for the same period of time. This procedure may be repeated to the point where the activity of the catalyst falls below a specified value. Fig. 10 shows the results of the stability assessment. Although the reused TS-50 shows a slightly poorer ODS performance compared to the fresh TS-50, it is still active and can achieve >99% sulfur removal in an hour during the second period. This behavior could be attributed to the highly dispersed surface active sites on TS-50, which helps retain its performance. During the third period, the ODS performance of the catalyst diminishes to a greater extent so that it can remove >99% of the sulfur compounds after 120 min. The decline in the performance of TS-50 can be ascribed to the accumulation of DBT and $DBTO_2$ molecules on the surface of the catalyst or pore blocking by polar molecules like water and *tert*-butyl alcohol. Table 3 compares the initial rates and rate constants of ODS reaction over TS-50 for different periods.

### 3.4. Evaluation of catalyst regenerability

As was discussed, the ODS catalyst deactivates over time. Since catalyst reusability is a key feature for its industrial application, we investigated the regenerability of the spent TS-50 catalyst. High temperature oxidation reaction was employed to regenerate the spent catalyst. At the end of the reaction, the catalyst was recovered by simple filtration, calcined at 873 K for 2 h, and then reused. As it is shown in Fig. 11, the regenerated catalyst was highly active and stable and it could remove DBT completely in an hour after two reaction–regeneration cycles. Apparently using a calcination temperature of 873 K resulted in oxidation and desorption of adsorbed sulfur species, especially sulfones. Consequently the catalyst retrieved its activity. It appears that at this temperature the catalyst microstructure is stable and its textural properties are not affected. However, the effect of the regeneration temperature on the long-term activity of the $TiO_2$–$SiO_2$ nanocomposite catalysts needs to be further investigated.

### 3.5. Effect of reaction temperature and kinetics of the ODS

Since TS-50 acts as both catalyst and adsorbent and generally the working temperature windows for catalysts and adsorbents are different, we investigated the effect of reaction temperature on the ODS efficiency. A series of experiments at different temperatures were conducted and the results are shown in Fig. 12. As it can be observed, increasing the temperature had a positive effect on the oxidative desulfurization of DBT. Higher reaction temperature increased the oxidation rate of DBT to DBT-sulfone and thus, increased the degree of sulfur removal. The ODS reaction

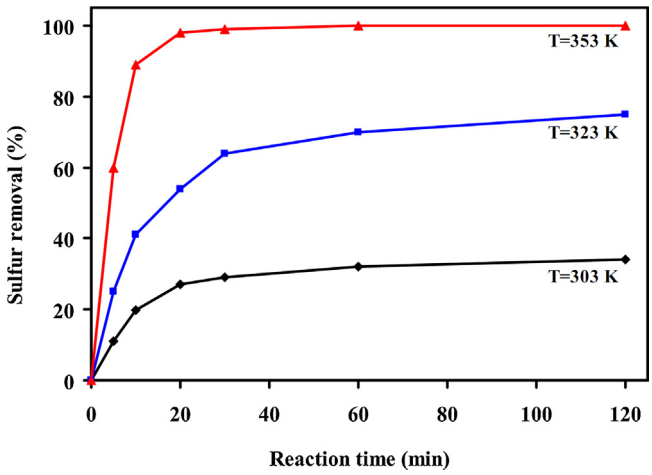


**Fig. 12.** Dependence of the DBT removal vs. reaction time on the ODS temperature over TS-50. Reaction condition: 20 g of model fuel (2875 ppmw DBT in isooctane), 0.2 g catalyst and TBHP:DBT molar ratio of 5.

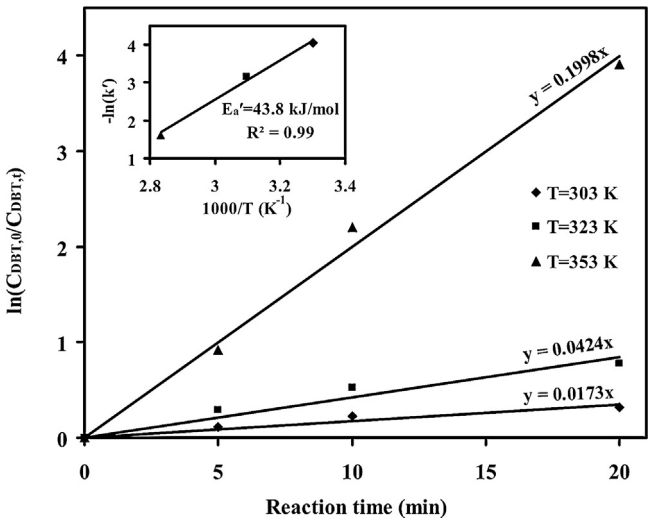


**Fig. 13.** Pseudo-first-order rate constants for DBT ODS reaction at 303 K, 323 K and 353 K over TS-50 (inset shows Arrhenius plot for DBT oxidation). Reaction condition: 20 g of model fuel (2875 ppmw DBT in isooctane), 0.2 g catalyst and TBHP:DBT molar ratio of 5.

could not be completed at 303 K and 323 K even after 120 min, but increasing the reaction temperature to 353 K led to a remarkable enhancement in the removal of sulfur compounds from 54 (percent sulfur removal at 323 K) to 98% after just 20 min. It should be mentioned that at temperatures higher than 353 K, the rate of thermal decomposition of TBHP becomes significant, which diminishes the concentration of the oxidant and consequently the efficiency of ODS process. Furthermore, liquid fuels are very complex mixtures and contain alkenes and aromatics. Performing the reaction at higher temperatures could enhance undesirable oxidation reactions of these compounds which in turn decreases the oil recovery. Results from the present study, indicated that 353 K is a favorable operating temperature for the ODS.

In order to study the kinetics of the oxidation of DBT it is assumed that adsorption of the unreacted DBT is much slower than its oxidation via the ODS reaction and the subsequent adsorption of the $DBTO_2$. The results obtained at different temperatures and at short reaction times, where most of the active sites of the catalyst are still available for the reactants, were used for this study.

The reaction mixture is a two phase slurry system in which the organic phase contains the reactant DBT and the oxidant TBHP and the catalyst TS-50 constitutes the solid phase. Water from the aqueous solution of TBHP is adsorbed into the catalyst pores.

The reaction may be written as DBT + 2 TBHP → $DBTO_2$ + 2 *tert*-butyl alcohol. An empirical kinetic model, Eq. (1) through Eq. (5), is assumed to predict the reaction rate in the absence of mass transfer limitations:

$$-\frac{d[C_{DBT}]}{dt} = k[C_{TBHP}]^m[C_{DBT}]^n \quad (1)$$

The amount of TBHP was in excess (TBHP:DBT molar ratio = 5) and the change in concentration of TBHP compared to the change in DBT concentration is negligible and therefore, the concentration of TBHP is considered to be constant. Hence, the reaction may be considered as pseudo first order for which the rate of the reaction may be expressed as

$$-\frac{d[C_{DBT}]}{dt} = k'[C_{DBT}]^n \quad (2)$$

where,

$$k' = k[C_{TBHP}]^m \quad (3)$$

$k'$ is the apparent rate constant. Eq. (2) has been integrated for $n = 1$, with the following boundary conditions:

$$t = 0, C_{DBT} = C_{DBT,0} \text{ and } t = t, C_{DBT} = C_{DBT,t} \quad (4)$$

integrating Eq. (2) yields:

$$\ln\left[\frac{C_{DBT,0}}{C_{DBT,t}}\right] = k't \quad (5)$$

where, $C_{DBT,0}$ and $C_{DBT,t}$ are the initial and instantaneous concentrations of DBT (or sulfur) respectively.

As it can be observed from Fig. 13, there is a linear relationship between $\ln(C_{DBT,0}/C_{DBT,t})$ and reaction time ($t$) for the oxidative desulfurization of DBT, confirming that ODS reaction follows pseudo first order kinetics in terms of sulfur concentration. The apparent rate constants ($k'$) at various temperatures were obtained from the slopes of the straight lines. Finally, the apparent activation energies were calculated from Arrhenius plots, shown in the inset of Fig. 13, and found to be 43.8 kJ/mol.

### 3.6. ODS reactivities of different sulfur compounds

In order to investigate the catalytic oxidation reactivities of different refractory sulfur compounds, the ODS of a model fuel composed of 167 ppmw S of each of BT, DBT, and 4,6-DMDBT in isooctane was conducted at 353 K over TS-50 nanocomposite. The conversions of the sulfur compounds vs. reaction time are shown in Fig. 14. The inset of Fig. 14 represents the ODS reactivities evaluated as pseudo-first-order rate constants ($k'_{ODS}$). The results showed that more than 98% conversions of DBT and 4,6-DMDBT were obtained after 20 and 30 min, respectively. BT was the most refractory sulfur compound in this system and >96% conversion was achieved after 120 min. The catalytic oxidation reactivities of the sulfur compounds was found to decrease in the order of DBT > 4,6-DMDBT > BT. The above results indicated that both electron density on sulfur atoms and the steric hindrance may play important roles in this ODS system. The lowest reactivity observed for BT is attributed to the significant lower electron density (5.696) on sulfur atom in BT compared with those in DBT (5.758) and 4,6-DMDBT (5.760). The difference in electron density on the sulfur atoms of DBT and 4,6-DMDBT is very small and can be ignored [70]. Therefore, the oxidation reactivity differences between DBT and 4,6-DMDBT could be ascribed to the steric hindrance caused by

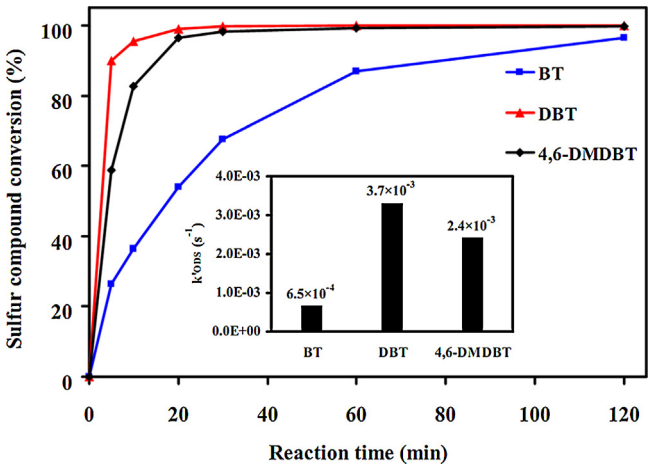


**Fig. 14.** ODS conversion of different sulfur compounds over TS-50 as a function of reaction time. Inset shows the ODS reactivities of BT, DBT, and 4,6-DMDBT evaluated as pseudo-first-order rate constants ($k'_{ODS}$). Reaction condition: 20 g of model fuel (167 ppmw S as BT + 167 ppmw S as DBT+167 ppmw S as 4,6-DMDBT in isooctane), 353 K, 0.2 g catalyst and TBHP:DBT molar ratio of 5.

methyl group at 4- and 6-positions in 4,6-DMDBT which makes the interaction of sulfur atom with the oxidant and/or catalyst active sites more difficult.

### 3.7. Theoretical calculations

XRD patterns (Fig. 4) show that the contribution of anatase (1 0 1) Miller plane is more predominant than the other Miller planes. It is believed that anatase titania in the equilibrium morphology displays primarily the (1 0 1) surface [71]. Amorphous silica has often been modeled as a surface of crystalline β-cristobalite [72,73]. Here we used (0 0 1) surface of β-cristobalite, which has shown to resemble amorphous silica very closely [73]. The surfaces were considered to be dehydrated corresponding to the high calcination temperature of the samples. The surface supercell dimensions (Å) were $a = 10.24$, $b = 27.00$, $c = 23.00$ with 17 Å of vacuum for the (1 0 1) plane of anatase titania and $a = 14.93$, $b = 14.93$, $c = 31.00$ with 24 Å of vacuum for the (0 0 1) plane of β-cristobalite.

After optimizing the geometries of DBT, $DBTO_2$ and TBHP molecules and anatase titania (1 0 1) and β-cristobalite (0 0 1) surfaces, the molecules were positioned above each surface with different starting orientations. The adsorbate–surface complexes with the most exothermic adsorption energies were selected as the optimized geometries. The adsorption energies ($\Delta E_{ads}$) were calculated for adsorbates on the clean surfaces using Eq. (6):

$$\Delta E_{ads} = E_{adsorbate-surface} - (E_{adsorbate} + E_{surface}) \quad (6)$$

where, $E_{adsorbate\text{-}surface}$ is the energy of adsorbate on the titania or silica surface in its fully relaxed state, $E_{adsorbate}$ and $E_{surface}$ are the energies of isolated molecule and optimized clean titania or silica surface, respectively. A negative value for adsorption energy implies an exothermic adsorption process with an attraction between molecule and surface.

The most stable adsorption configurations of the DBT, $DBTO_2$ and TBHP on the anatase titania (1 0 1) and β-cristobalite (0 0 1) surfaces are shown in Fig. 15, respectively, and the results for adsorption energies and related bond lengths are listed in Table 4.

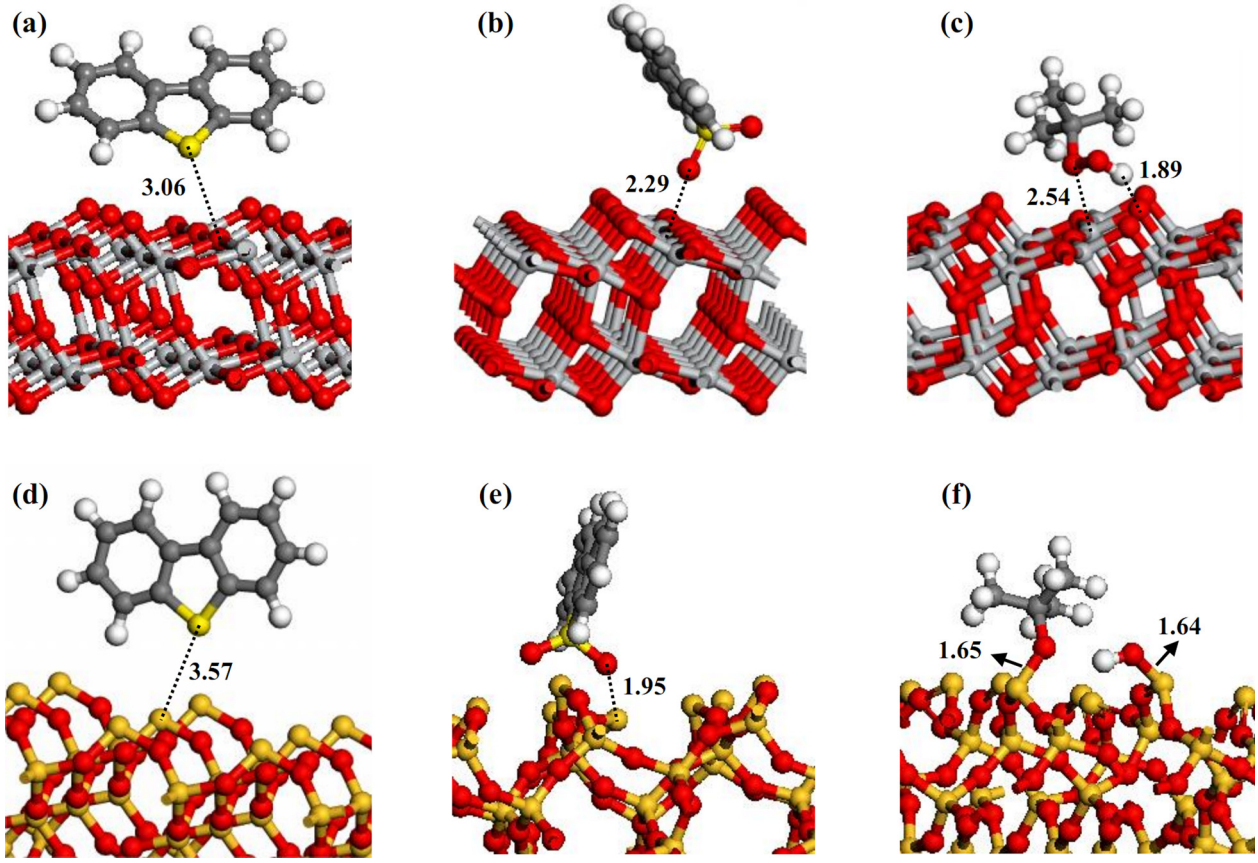


**Fig. 15.** Adsorption configurations of (a) DBT, (b) $DBTO_2$, (c) TBHP on anatase titania (1 0 1) surface and (d) DBT, (e) $DBTO_2$ and (f) TBHP on β-cristobalite (0 0 1) surface (bonding lengths are in Å). Red ball: oxygen, white ball: hydrogen, dark grey ball: carbon, light grey ball: titanium, dark yellow ball: silicon, light yellow ball: sulfur. (For interpretation of the references to color in this figure legend, the reader is referred to the web version of this article.)

**Table 4**
Adsorption energies and bonding lengths for the DBT, $DBTO_2$ and TBHP adsorbed on the anatase titania (1 0 1) and β-cristobalite (0 0 1) surfaces.

| Adsorbate | $TiO_2$ (1 0 1) | | β-cristobalite (0 0 1) | |
|---|---|---|---|---|
| | $\Delta E_{ads}$ (kcal/mol) | Adsorption bonding length (Å) | $\Delta E_{ads}$ (kcal/mol) | Adsorption bonding length (Å) |
| DBT | −3.4 | 3.06 | −5.1 | 3.57 |
| $DBTO_2$ | −6.2 | 2.29 | −29.6 | 1.95 |
| TBHP | −19.1 | 2.54 | −155.7 | 1.65[a] |

[a] Dissociative chemisorption.

In all optimized configurations, the S or O atom of DBT, $DBTO_2$ and TBHP are pointing toward the titania and silica surfaces. The plane of the aromatic rings may be characterized as a hydrophobic unit and is therefore tilted toward the surface. This shows that adsorption is dominantly through the interaction between the S and O atoms of the adsorbates and Ti or Si atoms on the corresponding surfaces. This may be of a great importance, when selectivity of catalyst/adsorbent in the presence of other types of hydrocarbons in fuels is considered.

The calculated $\Delta E_{ads}$ values show that both the anatase titania (1 0 1) and β-cristobalite (0 0 1) surfaces can adsorb DBT, $DBTO_2$ and TBHP. However, larger $\Delta E_{ads}$ values were obtained for adsorption of the adsorbates on the latter surface. Therefore, the adsorption of DBT, $DBTO_2$ and TBHP are stronger on the β-cristobalite (0 0 1) surface. The relative adsorption energies of the adsorbates on both anatase titania (1 0 1) and β-cristobalite (0 0 1) surfaces follow the order: TBHP ≫ $DBTO_2$ ≫ DBT. The adsorption energy of $DBTO_2$ is significantly larger than that of DBT. This increased binding strength for $DBTO_2$ arises from the two oxygen atoms of this molecule. For β-cristobalite (0 0 1) surface, we found a dissociative adsorption of TBHP ($\Delta E_{ads}$ = −155.7 kcal/mol). Such adsorption may decrease the concentration of oxidant in the reaction mixture and inhibit the ODS reaction. On the other hand, the adsorption energy of TBHP on anatase titania (1 0 1) surface is strong enough ($\Delta E_{ads}$ = −19.1 kcal/mol) to stabilize TBHP on the surface, but not too strong to decrease the concentration of this reactant. Based on our preliminary DFT calculations (not shown here), we think that the oxidation of DBT to DBTO, which apparently has the highest activation energy [74], is the rate determining step of the whole process. This could partially explain the lower specific activity observed for silica compared to titania. More computational studies are in progress to further elucidate the different catalytic activities observed for titania and silica. This DFT study is expected to serve as a guideline for an improved theoretical investigation of oxidative desulfurization of DBT family of refractory sulfur compounds.

## 4. Conclusions

Microporous $TiO_2$–$SiO_2$ nanocomposite catalysts-adsorbents were synthesized by a sol–gel method and used for ultra-deep oxidative desulfurization (ODS) of DBT.

Relationships between the structure and performance of these materials were elucidated. The results indicated that the structure, morphology and catalytic–adsorptive properties of the resulting $TiO_2$–$SiO_2$ nanocomposites were profoundly affected by the amount of titania. The titania crystallites were observed for the samples containing more than 25 wt% titania. The BET surface area increased with the nanocomposite silica contant, while the total acidity showed a maximum at 50 wt% titania. The catalyst with 50 wt% $TiO_2$ (TS-50) was found to exhibit the highest ODS activity of more than 98% sulfur removal to less than 10 ppmw S in 20 min. This has also been attributed to the significant dispersing effect of amorphous silica, resulting in a higher amount of Ti surface active species. In addition, it was shown that the micropores of TS-50, with the dimension of about 1.2 nm, were wide enough to make this catalyst highly active for the oxidation of bulky DBT (8 Å) to sulfoxide/sulfones without significant diffusion limitations.

The adsorption of DBT and highly polar DBT-sulfone and also polar water/*tert*-butyl alcohol on the surface of the TS-50 are responsible for catalyst deactivation. However, the catalyst could be regenerated by high temperature oxidation treatment with a negligible activity loss, indicating a high stability of the catalyst. Investigation of the kinetics of DBT ODS at short reaction times suggested that the oxidation reaction was pseudo first-order with apparent activation energy of 43.8 kJ/mol.

Density functional theory (DFT) calculations revealed that adsorption energy of $DBTO_2$ was significantly larger than DBT on both titania and silica surfaces. Moreover, TBHP was dissociatively adsorbed on the silica surface. This may decrease the concentration of the reactive oxidant species and the rate of ODS on silica.

## Acknowledgements

This work was supported by funding from the National Iranian Oil Refining & Products Distribution Company, Catalysis and the Nanostructured Materials Laboratory and Oil and Gas Center of Excellence at the University of Tehran.

## References

[1] C.S. Song, X.L. Ma, Appl. Catal. B-Environ. 41 (2003) 207–238.
[2] E. Lorençon, D.C.B. Alves, K. Krambrock, E.S. Avila, R.R. Resende, A.S. Ferlauto, R.M. Lago, Fuel 132 (2014) 53–61.
[3] Y. Xue-min, S. Gao-shen, X. Lin, J. Fuel Chem. Technol. 37 (2009) 318–323.
[4] A. Zhou, X.L. Ma, C.S. Song, Appl. Catal. B-Environ. 87 (2009) 190–199.
[5] C.S. Song, Catal. Today 86 (2003) 211–263.
[6] R. Wang, F. Yu, G. Zhang, H. Zhao, Catal. Today 150 (2010) 37–41.
[7] O. van Rheinberg, K. Lucka, H. Khne, T. Schade, J.T. Andersson, Fuel 87 (2008) 2988–2996.
[8] Y. Jia, G. Li, G. Ning, Fuel Process. Technol. 92 (2011) 106–111.
[9] O. Etemadi, T.F. Yen, Energy Fuels 21 (2007) 2250–2257.
[10] A.D. Giuseppe, M. Crucianelli, F.D. Angelis, C. Crestini, R. Saladino, Appl. Catal. B-Environ. 89 (2009) 239–245.
[11] O.G. Garca, L.C. Caero, Catal. Today 148 (2009) 42–48.
[12] M.W. Wan, T.F. Yen, Appl. Catal. A-Gen. 319 (2007) 237–245.
[13] V.V.D.N. Prasad, K.E. Jeong, H.J. Chae, C.U. Kim, S.Y. Jeong, Catal. Commun. 9 (2008) 1966–1969.
[14] J.L.G. Gutiérrez, G.A. Fuentes, M.E.H. Terán, F. Murrieta, J. Navarrete, F.J. Cruz, Appl. Catal. A-Gen. 305 (2006) 15–20.
[15] L.C. Caero, E. Hernández, F. Pedraza, F. Murrieta, Catal. Today 107–108 (2005) 564–569.
[16] C.S. Shalaby, S.K. Saha, X. Ma, C.S. Song, Appl. Catal. B-Environ. 101 (2011) 718–726.
[17] O. Etemadi, T.F. Yen, J. Colloid Interface Sci. 313 (2007) 18–25.
[18] D. Wang, E.W. Qian, H. Amano, K. Okata, A. Ishihara, T. Kabe, Appl. Catal. A-Gen. 253 (2003) 91–99.
[19] X. Zhou, J. Li, X. Wang, K. Jin, W. Ma, Fuel Process. Technol. 90 (2009) 317–323.
[20] N.Y. Chan, T.Y. Lin, T.F. Yen, Energy Fuels 22 (2008) 3326–3328.
[21] G. Yu, S. Lu, H. Chen, Z. Zhu, Energy Fuels 19 (2005) 447–452.
[22] M.F. Ali, A. Al-Malki, S. Ahmed, Fuel Process. Technol. 90 (2009) 536–544.
[23] M. Te, C. Fairbridge, Z. Ring, Appl. Catal. A-Gen. 219 (2001) 267–280.
[24] H.G. Bernal, L.C. Caero, A.G. Alejandre, Catal. Today 142 (2009) 227–233.
[25] B. Zapata, F. Pedraza, M.A. Valenzuela, Catal. Today 106 (2005) 219–221.
[26] A. Ishihara, D. Wang, F. Dumeignil, H. Amano, E.W. Qian, T. Kabe, Appl. Catal. A-Gen. 279 (2005) 279–287.
[27] L. Yang, J. Li, X. Yuan, J. Shen, Y. Qi, J. Mol. Catal. A: Chem. 262 (2007) 114–118.
[28] A. Chica, A. Corma, M.E. Dmine, J. Catal. 242 (2006) 299–308.
[29] L. Kong, G. Li, X. Wang, Catal. Today 9395 (2004) 341–345.
[30] L.F. Mijangos, L.C. Caero, Ind. Eng. Chem. Res. 50 (2011) 2659–2664.

[31] L.F.R. Verduzco, E.T. García, R.G. Quintana, V.G. Peña, F.M. Guevara, Catal. Today 98 (2004) 289–294.
[32] L.C. Caero, H.G. Bernal, A.F. Cuevas, H.D.G. Gomez, R.C. Garcia, Catal. Today 133–135 (2008) 244–254.
[33] E. Torres-García, A. Galano, G. Rodriguez-Gattorno, J. Catal. 282 (2011) 201–208.
[34] C. Jin, G. Li, X. Wang, Y. Wang, L. Zhao, D. Sun, Micropor. Mesopor. Mater. 111 (2008) 236–242.
[35] K.S. Cho, Y.K. Lee, Appl. Catal. B-Environ. 147 (2014) 35–42.
[36] A.T. Shah, B. Li, Z.E.A. Abdalla, J. Colloid Interface Sci. 336 (2009) 707–711.
[37] C. Jin, G. Li, X. Wang, L. Zhao, L. Liu, H. Liu, Chem. Mater. 19 (2007) 1664–1670.
[38] V. Hulea, F. Fajula, J. Bousquet, J. Catal. 198 (2001) 179–186.
[39] C. Shifu, L. Yueming, G. Jinbao, W. Lingling, L. Xiuli, G. Guohua, W. Peng, H. Mingyuan, Chin. J. Catal. 27 (2006) 547–549.
[40] Q. Lv, G. Li, H. Sun, Fuel 130 (2014) 70–75.
[41] R. Hutter, T. Mallat, A. Baiker, J. Chem. Soc. Chem. Commun. (1995) 2487–2488.
[42] X. Gao, I.E. Wachs, Catal. Today 51 (1999) 233–254.
[43] Y. Kato, N. Matsushita, H. Yoshida, T. Hattori, Catal. Commun. 3 (2002) 99–103.
[44] C. Su, B.Y. Hong, C.M. Tseng, Catal. Today 96 (2004) 119–126.
[45] D.C.M. Dutoit, M. Schneider, A. Baiker, J. Catal. 153 (1995) 165–176.
[46] R. Mariscal, M.L. Granados, C. Martos, J.L.G. Fierro, J.L. Sotelo, C. Martos, R. van Grieken, Langmuir 16 (2000) 9460–9467.
[47] X. Ma, S. Velu, J.H. Kim, C.S. Song, Appl. Catal. B-Environ. 56 (2005) 137–147.
[48] S. Baroni, A.D. Corso, S.D. Gironcoli, P. Giannozzi, C. Cavazzoni, G. Ballabio, S. Scandolo, G. Chiarotti, P. Focher, A. Pasquarello, K. Laasonen, A. Trave, R. Car, N. Marzari, A. Kokalj, http://www.pwscf.org/
[49] J.P. Perdew, K. Burke, M. Ernzerhof, Phys. Rev. Lett. 77 (1996) 3865–3868.
[50] S. Nair, B.J. Tatarchuk, Fuel 89 (2010) 3218–3225.
[51] X.M. Yan, P. Mei, J. Lei, Y. Mi, L. Xiong, L. Guo, J. Mol. Catal. A: Chem. 304 (2009) 52–57.
[52] S. Nair, A.H.M. Shahadat Hussain, B.J. Tatarchuk, Fuel 105 (2013) 695–704.
[53] A.H.M. Shahadat Hussain, B.J. Tatarchuk, Fuel 107 (2013) 465–473.
[54] K. Castillo, J.G. Parsons, D. Chavez, R.R. Chianelli, J. Catal. 268 (2009) 329–334.
[55] K.Y. Jung, S.B. Park, Appl. Catal. B-Environ. 25 (2000) 249–256.
[56] C. Su, K.F. Lin, Y.H. Lin, B.H. You, J. Porous Mater. 13 (2006) 251–258.
[57] J. Bu, G. Loh, C.G. Gwie, S. Dewiyanti, M. Tasrif, A. Borgna, Chem. Eng. J. 166 (2011) 207–217.
[58] D.H. Everett, J.C. Powl, J. Chem. Soc. Faraday Trans. 172 (1976) 619–636.
[59] R.G. Rodríguez Avendaño, J.A. De Los Reyes, T. Viveros, J.A. Montoya De La Fuente, Catal. Today 148 (2009) 12–18.
[60] Z. Li, B. Hou, Y. Xu, D. Wu, Y. Sun, W. Hu, F. Deng, J. Solid State Chem. 178 (2005) 1395–1405.
[61] R.J. Davis, Z. Liu, Chem. Mater. 9 (1997) 2311–2324.
[62] J. Dou, H.C. Zeng, ACS Catal. 4 (2014) 566–576.
[63] M. Massa, A. Andersson, E. Finocchio, G. Busca, J. Catal. 307 (2013) 170–184.
[64] S. Imamura, T. Shiomi, S. Ishida, K. Utani, H. Jindai, Ind. Eng. Chem. Res. 29 (1990) 1758–1761.
[65] M. Kobayashi, R. Kuma, S. Masaki, N. Sugishima, Appl. Catal. B-Environ. 60 (2005) 173–179.
[66] Z. Liu, J. Tabora, R.J. Davis, J. Catal. 149 (1994) 117–126.
[67] B. Notari, R.J. Willey, M. Panizza, G. Busca, Catal. Today 116 (2006) 99–110.
[68] S. Hu, R.J. Willey, B. Notari, J. Catal. 220 (2003) 240–248.
[69] G. Rodriguez-Gattorno, A. Galano, E. Torres-García, Appl. Catal. B-Environ. 92 (2009) 1–8.
[70] H. Lü, W. Ren, H. Wang, Y. Wang, W. Chen, Z. Suo, Appl. Catal. A-Gen. 453 (2013) 376–382.
[71] S. Dzwigaj, C. Arrouvel, M. Breysse, C. Geantet, S. Inoue, H. Toulhoat, P. Raybaud, J. Catal. 236 (2005) 245–250.
[72] S.A. Mian, L.C. Saha, J. Jang, L. Wang, X. Gao, S. Nagase, J. Phys. Chem. C 114 (2010) 20793–20800.
[73] J. Handzlik, R. Grybos, F. Tielens, J. Phys. Chem. C 117 (2013) 8138–8149.
[74] X. Zeng, G. Mo, H. Wang, R. Zhou, C. Zhao, Comput. Theor. Chem. 1037 (2014) 22–27.